iScience

CellPress
OPEN ACCESS

Article

Treatment of calcific arterial disease via enhancement of autophagy using GSK343

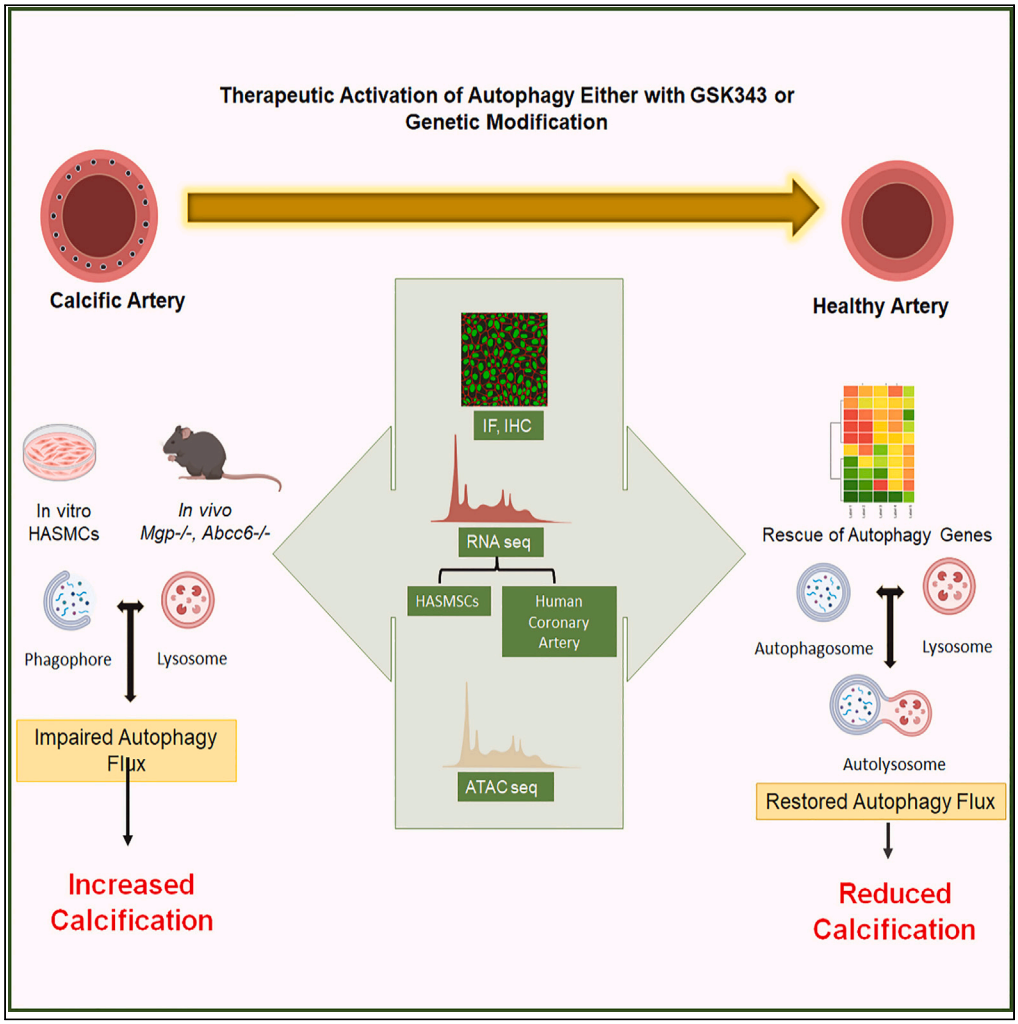

Christian L. Lino Cardenas, Wanlin Jiang, Lova P. Kajuluri, ..., Zhixun Dou, Clint L. Miller, Rajeev Malhotra

Clinocardenas@mgh.harvard.edu (C.L.L.C.)
rmalhotra@mgh.harvard.edu (R.M.)

Highlights

Impaired autophagy initiation is a determinant of vascular calcification

Chromatin rearrangement at autophagy genes in calcified VSMCS

Chromatin relaxation by GSK343 restores autophagy initiation gene expression

Pharmacologic or genetic enhancement of autophagy inhibits vascular calcification

Lino Cardenas et al., iScience *26*, 108360
November 17, 2023
https://doi.org/10.1016/j.isci.2023.108360

iScience

CellPress
OPEN ACCESS

Article

Treatment of calcific arterial disease via enhancement of autophagy using GSK343

Christian L. Lino Cardenas,[1,9,*] Wanlin Jiang,[1,9] Lova P. Kajuluri,[1] Kuldeep Singh,[1] Katrina Ostrom,[1] Rebecca Li,[1] Francois Cherbonneau,[1] Sophie Boerboom,[1] Claire Birchenough,[1] Kangsan Roh,[1] Elizabeth L. Chou,[1,2] Zarbafian Shahrooz,[1] Christopher Nicholson,[1] Adam L. Johnson,[1] Sujin Lee,[1] Fumito Ichinose,[3] Donald B. Bloch,[3,4] Sagar Nigwekar,[5] Patrick T. Ellinor,[1] Patricia Musolino,[6] Mark E. Lindsay,[1] Zhixun Dou,[8] Clint L. Miller,[7] and Rajeev Malhotra[1,10,*]

SUMMARY

Vascular calcification is a hallmark of atherosclerotic disease and serves as a strong predictor and risk factor for cardiovascular events. Growing evidence suggests that autophagy may play a protective role in early atherosclerosis. The precise effects of autophagy on VSMC-mediated calcification remain unknown. In this study, we utilized multi-omic profiling to investigate impaired autophagy at the transcriptional level as a key driver of VSMC calcification. Our findings revealed that impaired autophagy is an essential determinant of VSMC calcification. We observed that an osteogenic environment affects the open chromatin status of VSMCs, compromising the transcriptional activation of autophagy initiation genes. *In vivo* experiments involve pharmacological and genetic activation of autophagy using mouse models of spontaneous large (*Mgp*$^{-/-}$) and small (*Abcc6*$^{-/-}$) artery calcification. Taken together, these data advance our mechanistic understanding of vascular calcification and provide important insights for a broad range of cardiovascular diseases involving VSMC phenotype switch.

INTRODUCTION

The mature vascular smooth muscle cell (VSMC) is not terminally differentiated and exhibits remarkable plasticity even during adulthood.[1] Intimal and medial arterial calcification are characterized by the transdifferentiation or phenotypic transition of VSMCs from contractile cells to proliferative, osteogenic cells.[2,3] During the course of vascular calcification, VSMC phenotypic transition is associated with both a loss of the contractile apparatus and an increase in osteogenic markers such as Runt-related transcription factor 2 (RUNX2) and alkaline phosphatase (ALPL).[4,5] Runx2 is a master transcriptional regulator that is required for VSMC phenotypic transition and osteogenic activity.[6] VSMCs undergoing phenotypic transition within atherosclerotic lesions migrate into the intima, where they proliferate, produce calcified extracellular matrix, and participate in fibrous cap formation that alters plaque stability.[1] The process of VSMC phenotype transition contributes to a range of vascular pathologies including vascular calcification, atherosclerosis, calciphylaxis, vascular restenosis, transplant vasculopathy, and arterial stiffness.[6–8]

Autophagy is an evolutionarily conserved, tightly regulated process through which eukaryotic cells recycle cellular components and deliver unnecessary or potentially dangerous cellular materials in double-membrane vesicles for degradation via fusion with lysosomal compartments.[9–11] Autophagy consists of multiple steps including autophagosome initiation and nucleation, elongation, lysosomal fusion to create autolysosomes, and degradation. Specifically, autophagy initiation/nucleation is characterized by the formation of the autophagy-initiation complex (or ULK1 complex),[12] and this early phase of autophagy is dependent on multiple factors including ULK1, ULK2, ATG101, ATG12, ATG13, PIK3R3, ATG5, ATG7, ATG14, ATG16L1/L2, FIP200 (aka *RB1CC1*), BECN1, VPS34, and VPS13A.[13,14] Autophagic flux is a term used to describe the rate of autophagy-mediated degradation,[15] and impaired autophagic flux can be determined by multiple techniques including assessment of autophagic vacuole accumulation, disrupted autophagosome membrane integrity and/or lack of lysosomal fusion

[1]Cardiovascular Research Center, Cardiology Division, Department of Medicine, Massachusetts General Hospital, Harvard Medical School, Boston, MA, USA
[2]Division of Vascular and Endovascular Surgery, Massachusetts General Hospital, Boston, MA 02114, USA
[3]Department of Anesthesia, Critical Care and Pain Medicine at Massachusetts General Hospital, Boston, MA 02114, USA
[4]Division of Rheumatology, Allergy, and Immunology, Department of Medicine, Massachusetts General Hospital, Boston, MA 02114, USA
[5]Division of Nephrology, Department of Medicine, Massachusetts General Hospital, Boston, MA 02114, USA
[6]Department of Neurology, Massachusetts General Hospital, Harvard Medical School, Boston, MA 02114, USA
[7]Center for Public Health Genomics, Department of Public Health Sciences, University of Virginia, Charlottesville, VA 22908, USA
[8]Center for Regenerative Medicine, Massachusetts General Hospital, Harvard Medical School, Boston, MA 02114, USA
[9]These authors contributed equally
[10]Lead contact
*Correspondence: Clinocardenas@mgh.harvard.edu (C.L.L.C.), rmalhotra@mgh.harvard.edu (R.M.)
https://doi.org/10.1016/j.isci.2023.108360

on transmission electron microscopy (TEM), levels of autophagic protein LC3II and lack of co-localization with lysosomal proteins (i.e., LAMP1), accumulation of autophagic substrate SQSTM1 (also known as p62), and changes in the fluorescent signal of mRFP-GFP-LC3 reporter (as detailed later). Autophagy is essential for maintaining normal vascular cell homeostasis and function[14,16] and is considered protective during early atherosclerosis but can become dysregulated with advanced atherosclerosis.[11,17] We therefore aimed to ascertain the changes that occur in autophagy and the expression of autophagy-related genes in the context of VSMC osteogenic switch and calcification as well as in human and mouse models of vascular diseases of calcification.

RESULTS

Impaired autophagy is a determinant of VSMC calcification

To gain insights into the molecular mechanisms of VSMC calcification, we first performed RNA-seq analysis in VSMCs cultured in normal conditions and in media that promotes calcification (osteogenic media). Differential expression analyses revealed 3,657 upregulated and 3,738 downregulated genes under osteogenic conditions (Figure 1A). Pathway analyses of differentially expressed genes revealed enrichment of signaling pathways related to autophagy, including p53 and mTOR signaling, which are involved in autophagy signaling (Figure 1B). Based on the RNA-seq pathway analysis, we sought to determine the specific components of the autophagy pathway that are impaired in VSMC calcification. Data from RNA-seq analysis (Figure 1C) and subsequent protein and mRNA validation (Figures 1D and S1A) demonstrated that *ULK1* was significantly down-regulated among the autophagy-related genes in calcification. Importantly, ULK1 is required for the formation of the activation complex of autophagy, indicating that a defect in autophagy initiation may be a hallmark of calcified VSMCs. The down-regulation in autophagic initiation genes was associated with both VSMC calcification (alizarin red stain) and phenotypic switch as evidenced by decreased contractile protein expression (calponin, CNN1; SM22α) and increased RUNX2 (Figure 1D).

In further evaluation, immunoblot analyses of autophagy flux using chloroquine showed decreased lipidation of LC3 and increased accumulation of SQSTM1 (or p62, a substrate of autophagosomes), suggesting a disruption of autophagic flux in calcified VSMCs (Figure 1E). Furthermore, in immunofluorescence analyses, ULK1 protein expression was reduced and exhibited abnormal cytoplasmic localization compared with healthy VSMCs (Figure S1B), indicating a defect in the initiation step of the autophagy pathway and the capacity of ULK1 to appropriately interact with other members of the autophagy initiation complex. Taken together, these *in vitro* results demonstrate that VSMC calcification is associated with a defect in autophagy flux associated with a reduction in expression of genes required for the initiation of autophagy.

Because ULK1 is a critical component of the complex that initiates autophagosome formation, we sought to determine the effects of inhibiting ULK1 activity on VSMC calcification. Incubation of VSMCs in osteogenic media with SBI0206965,[18] a specific ULK1 inhibitor, increased calcification of VSMCs in a dose-dependent manner (Figure 1F). In contrast, activation of autophagy with rapamycin prevented VSMC calcification. Furthermore, in *ex vivo* analysis of wild-type mouse aortas treated with or without SBI0206965 under osteogenic conditions, ULK1 inhibition dramatically exacerbated aortic calcification as evidenced by increased OsteoSense signal, alizarin red staining, MMP activity, and Runx2 expression (Figure 1G).

Differential expression of autophagy initiation genes in vascular calcification was further underscored by *in situ* hybridization analysis of human aortic sections with atherocalcific disease as well as dermal biopsies from patients with calciphylaxis. Aortic calcification represents large vessel disease, whereas calciphylaxis is a disease characterized by rapidly progressive arteriolar calcification in adipose and skin tissue.[19] Interestingly, both types of calcification exhibit similar underlying molecular mechanisms. We observed that, both in aortic calcification (Figure 1H, upper panel) and in calciphylaxis (Figure 1H, lower panel and S1C), the presence of arterial calcification was associated with reduced ULK1 and ATG13A mRNA and protein levels compared with healthy, non-calcified control tissues.

Overall, our results show that VSMC calcification is characterized by the accumulation of autophagy substrate p62, indicating an impairment of autophagy flux. Furthermore, the gene expression results implicate a defect in the initiation of autophagy underlying VSMC calcification and that inhibition of the autophagy ULK1-initiation complex exacerbates osteogenic VSMC phenotype switching.

Differential expression of autophagy-initiation genes is associated with human coronary artery disease

To investigate the regulation of autophagy genes in human calcific atherosclerotic disease, we queried differential gene expression in a transcriptomic dataset derived from normal and ischemic human coronary artery tissues. The autophagy pathway was significantly enriched in downregulated genes (ischemic versus normal) using the KEGG ($p = 0.0114$) and WikiPathways ($p = 0.0011$) databases. A heat map for autophagy-related gene expression in ischemic versus normal human coronary tissue (ischemic versus normal) is presented in Figure S2A. Directional trends of gene expression were particularly similar for autophagy initiation genes in both the *in vitro* and coronary tissue RNA-seq analyses (Figure 2A). We identified 5 autophagy initiation genes of those listed earlier (*ATG12*, *ATG13*, *ATG16L1*, *BECN1*, and *VPS13A*) that were downregulated in ischemic, compared with normal, coronary arteries and 2 autophagy initiation genes (*ATG7* and *ATG16L2*) that were upregulated (Figure 2A and Table S1). *ULK1* gene expression levels were reduced in ischemic coronary arteries (Figure 2B), although this difference was only significant when adjusting for a minimal set of covariates (P-adj = 0.019). We next investigated genetic associations of autophagy initiation genes with vascular disease by performing summary-based Mendelian randomization (SMR) analysis of thoracic aortic calcification (TAC) genome-wide association study (GWAS) loci using expression quantitative trait loci (eQTL) from atherosclerotic aortic root and mammary artery tissues in the Stockholm-Tartu Atherosclerosis Reverse Networks

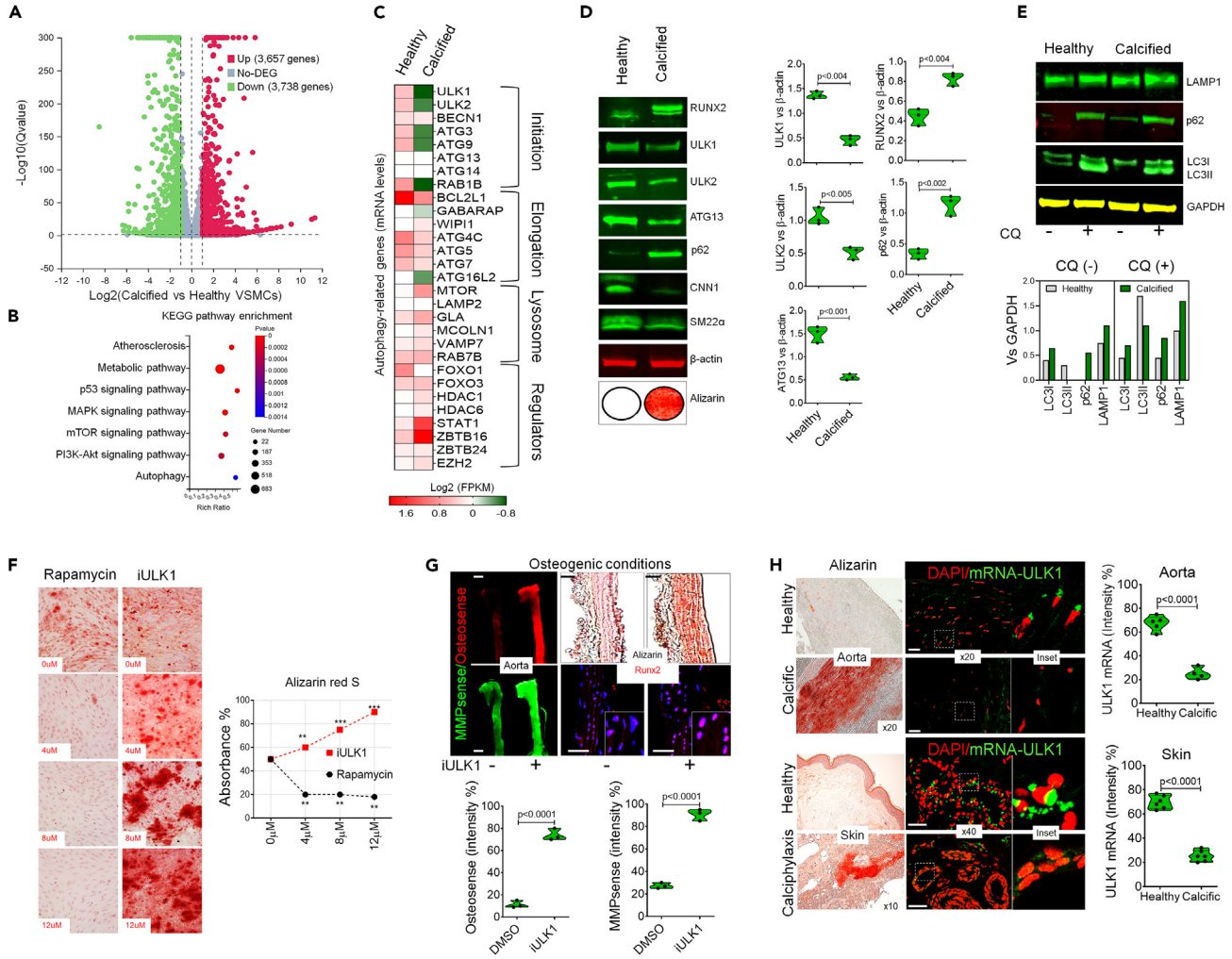

Figure 1. Impaired autophagy is a determinant of VSMC calcification

(A) RNA sequencing differential gene expression analysis for calcified versus healthy human VSMCs. Calcified VSMCs were grown in osteogenic media for 3 days.

(B) Analysis of canonical pathways impacted by global transcriptomic differential gene expression in calcified VSMCs.

(C) Heat map of mRNA expression of autophagy-related genes in healthy versus calcified VSMCs.

(D) Quantitative western blot analysis of calcification (RUNX2), autophagy initiation proteins (ULK1, ULK2, ATG13 and p62), and VSMC contractile (CNN1, SM22α) markers along with alizarin red stain for calcium.

(E) Quantitative western blot analysis of autophagy flux markers in calcified versus healthy VSMCs in the presence or absence of chloroquine (CQ).

(F) Alizarin red staining of human VSMCs under osteogenic conditions indicates calcification is inhibited in cells treated with rapamycin (autophagy activator) and is increased in cells treated with a ULK1 inhibitor (SBI-0206965; autophagy inhibition).

(G) (Left panel) *Ex vivo* treatment of mouse aortas with ULK1 inhibitor shows increased calcification (OsteoSense, red) and inflammation as measured by MMP activity (MMPsense, green). Right panel shows increased calcium deposition in aortas treated with ULK1 inhibitor (alizarin red staining) under osteogenic conditions and increased nuclear Runx2 signal (red) as assessed by immunofluorescence.

(H) Alizarin red staining and *in situ* hybridization for ULK1 mRNA (green) in fixed human tissue from aortic calcification and calciphylaxis patients were compared with healthy tissue, demonstrating reduced ULK1 mRNA levels in the setting of large and small vessel calcification. Significance was calculated using 1-way ANOVA with a Tukey's multi-comparisons test. Scale bars = 50 um.

Engineering Task (STARNET) dataset.[20] Integration of the GWAS and eQTL signals identified *ULK2* and *VPS13A* as the most likely autophagy effector genes whose expression is associated with TAC risk (Table S2). To complement these results, we leveraged genome-wide epigenomic profiles in coronary artery tissues and smooth muscle cells to determine enhancer-gene activity-by-contact (ABC) scores for disease-associated variants. This analysis identified *ATG16L2* as a likely effector gene of peripheral artery disease (PAD)-associated regulatory variants from the Million Veteran Program[8] (Figure 2B and Table S3). Taken together, these integrative analyses provide human genetic evidence for abnormal expression of autophagy-related genes involved in autophagosome initiation in the context of vascular disease.

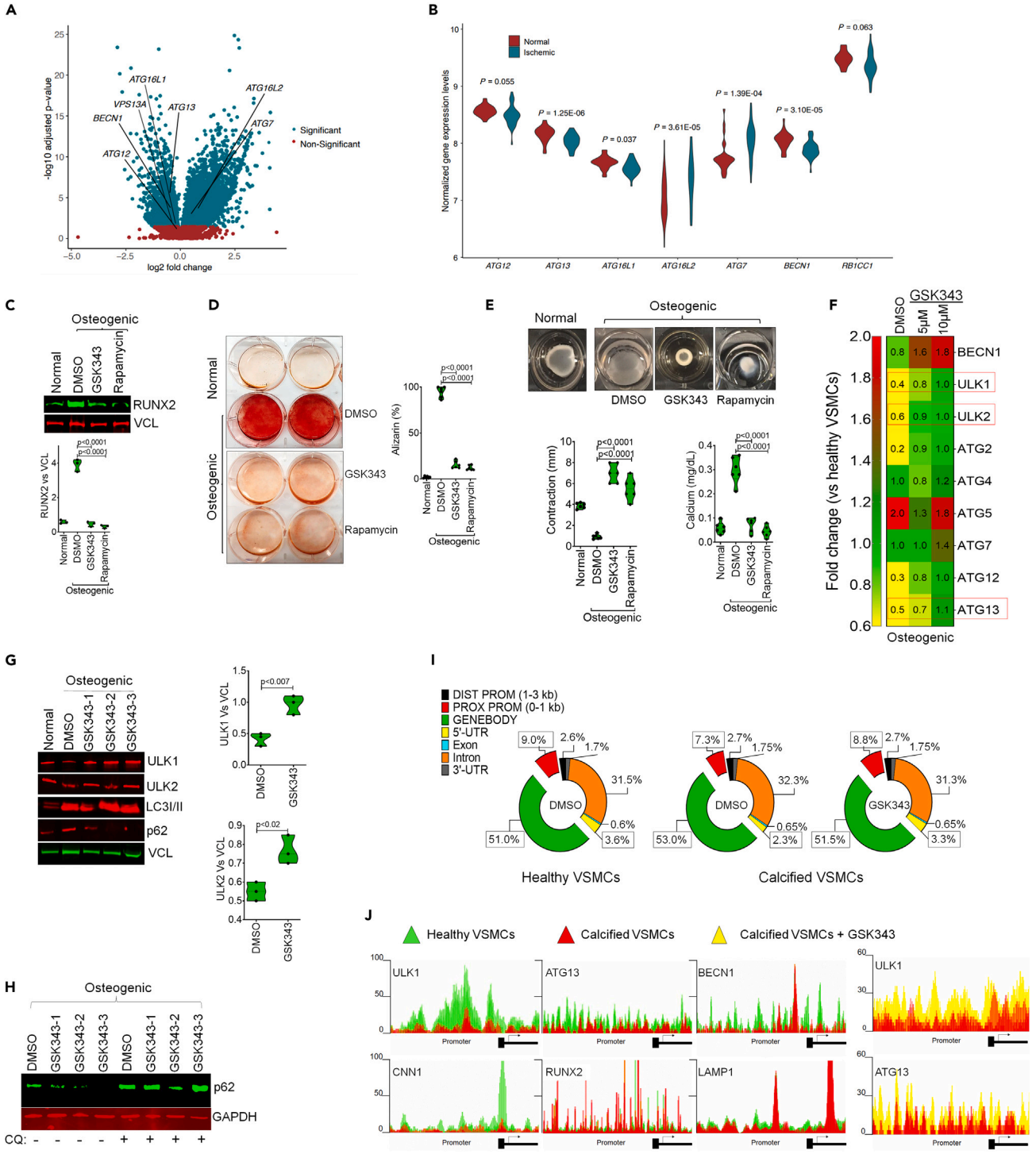

Figure 2. Differential expression of autophagy initiation genes is associated with human coronary artery disease, and therapeutic activation of autophagy inhibits vascular calcification

(A) Volcano plot of differentially expressed genes in normal (n = 24) versus ischemic (n = 36) human coronary artery tissues as detected using DESeq2. Significant differentially expressed genes were considered using FDR adjusted p value <0.05, as indicated by the green points. Autophagy genes are labeled with human gene symbols.

Figure 2. *Continued*

(B) Violin plots of differentially regulated autophagy genes in normal versus ischemic coronary artery tissues. Values represent log_{10} normalized gene expression levels quantified using a collapsed gene model and RNA-SeQC. p values shown are derived from DESeq2 analysis in normal (n = 24) versus ischemic (n = 36) human coronary artery samples.

(C) Immunoblot analysis of RUNX2 from total lysates of human VSMCs under normal or osteogenic conditions with or without treatment of autophagy activator (either GSK343 or rapamycin).

(D) Treatment with either GSK343 (10 μM) or rapamycin (100 nM), activators of autophagy, inhibited the calcification of human VSMCs grown in calcification media for 10 days, as evidenced by alizarin red stain.

(E) Collagen gel contraction assay was performed demonstrating that autophagy activation with either GSK343 or rapamycin restores the contractility of VSMCs that is disrupted when grown in osteogenic media and decreases cellular calcium content (mg/dL) by colorimetric cresolphthalein method.

(F) Heat map of the fold change in mRNA levels of autophagy-related genes from human VSMCs grown under osteogenic media treated without or with GSK343 at low (5 μM) or high (10 μM) concentrations compared with VSMCs in normal media.

(G) Immunoblot analysis of ULK1, ULK2, p62, and LC3BI/II from total lysates of human VSMCs under normal or osteogenic conditions and treated with GSK343 (10 μM with three replicates).

(H) Quantitative western blot analysis of autophagy flux markers in calcified versus healthy VSMCs shows decreased p62 protein in GSK343-treated cells.

(I) Pie chart showing the genomic distribution of the differentially accessible chromatin regions from human healthy VSMCs (top panel, left chart), calcified VSMCs (middle chart), and calcified VSMCs treated with GSK343 (right chart).

(J) Overlapping ATAC-seq tracks of the promoter regions of the autophagy-initiation genes (ULK1, ATG13A, BECN1), the contractile gene (CNN1), the calcification marker (RUNX2), and the lysosome marker (LAMP1). ATAC-seq peaks for healthy VSMCs are presented in green and for calcified VSMCs in red. The ATAC-seq data have been normalized to take depth into account, and the scale on the y axis was chosen for optimal visualization of peaks. Also, representative ATAC-seq tracks of the autophagy-initiation genes (ULK1 and ATG13A) from VSMCs under osteogenic conditions treated with DMSO (red peaks) or GSK343 (yellow peaks) are presented. Shown are a portion of the promoter regions (1-2Kb). Significance was calculated using 1-way ANOVA with a Tukey's multi-comparisons test. Scale bars = 50 um.

Therapeutic activation of autophagy inhibits vascular calcification

EZH2 has been described as a negative epigenetic regulator of autophagy by promoting the hypermethylation of the ATG5 and ATG7 genomic loci and through an MTOR-dependent pathway.[21,22] In agreement with previous reports, our RNA-seq data in the cellular model of vascular calcification also showed up-regulation of EZH2, which is associated with down-regulation of autophagy-related genes. The up-regulation of EZH2 further supports the choice of GSK343, which is a potent inhibitor of EZH2 catalytic activity. To determine if activation of autophagy improves vascular calcification and prevents VSMC phenotype switch *in vitro*, we used two activators of autophagy, GSK343 (an inhibitor of enhancer of zeste homolog 2, EZH2) and rapamycin (an mTOR inhibitor).[23] Activation of autophagy with GSK343 or rapamycin was associated with reduced RUNX2 protein levels (a master transcriptional activator of VSMC calcification) (Figure 2C). Treatment of VSMCs under osteogenic conditions with either GSK343 or rapamycin inhibited calcification by >80%, as determined by alizarin red staining (Figure 2D) and the cresolphthalein method for calcium quantification (Figures 2D and S2B) and preserved a normal contractile phenotype of VSMCs grown in osteogenic conditions (Figures 2E and S2C). Treatment of VSMCs under osteogenic conditions with GSK343 rescued the mRNA (Figure 2F) and protein (Figure 2G) expression of autophagy-initiation genes, most notably a dose-dependent increase in ULK1 with GSK343 treatment. Remarkably, GSK343 treatment of VSMCs under osteogenic conditions resolved the accumulation of p62 in calcification, indicating the restoration of autophagy flux (Figures 2G and 2H).

Given that GSK343 alters chromatin structure via inhibition of EZH2 catalytic activity (histone trimethylation), we sought to determine if the inhibition of calcification observed with GSK343 occurs via altering chromatin accessibility at key autophagy-related and calcification genes using ATAC-seq (assay for transposase accessible chromatin combined with high-throughput DNA sequencing).[24] Compared with normal VSMCs, calcified VSMCs exhibited a ~3% rearrangement of chromatin organization with specifically a loss of chromatin accessibility at proximal promoter and 5′ UTR regions, which was restored to more normal levels when treated with GSK343 (Figures 2I and S2D). In assessing the promoter regions of specific autophagy-initiation genes as well as contractile and calcification genes, promoter accessibility was significantly reduced at the *ULK1*, *ATG13A*, and *BECN1* (autophagy-initiation) and *CNN1* (contractile protein) promoters and increased at the *RUNX2* (calcification) promoter in calcified VSMCs compared with normal VSMCs. Interestingly, treatment of VSMCs in osteogenic media with GSK343 augmented chromatin accessibility in the promoter regions of ULK1 and ATG13A (Figure 2J). Altogether, these data point toward an important epigenetic regulation of autophagy-initiation genes with downstream effects on mRNA expression in VSMC calcification and identifies GSK343 as a novel inhibitor of VSMC calcification.

To corroborate the therapeutic potential of GSK343 in vascular calcification, we assessed (1) *ex vivo* human tissue samples from calcified aortas (and from healthy controls) and (2) dermal biopsies from end-stage kidney disease (ESKD) patients afflicted with calciphylaxis (and control patients with ESKD but not calciphylaxis). Immunofluorescence analysis of fixed tissues demonstrated reduced protein expression of ULK1 and the contractile protein CNN1 in calcified aortae (Figure 3A, left panel) and arterioles of calciphylaxis patients (Figure 3A, right panel) compared with their respective control samples. Using fresh (living) tissue samples, aortas and dermal biopsies from individual patients were sectioned and incubated in osteogenic conditions for 14 days in the presence or absence of GSK343 followed by fixation and histologic analysis. Treatment of *ex vivo* human aortic samples (Figure 3B) and calciphylaxis samples (Figure 3C) with GSK343 inhibited calcification induced by osteogenic media, and this reduction in calcification was associated with increased ULK1 and CNN1 protein levels by immunofluorescence. Taken together, our results point to GSK343 as a potent inhibitor of VSMC calcification through downstream transcriptional effects on autophagy initiation genes, perhaps in part through epigenetic regulation (Figure 3D).

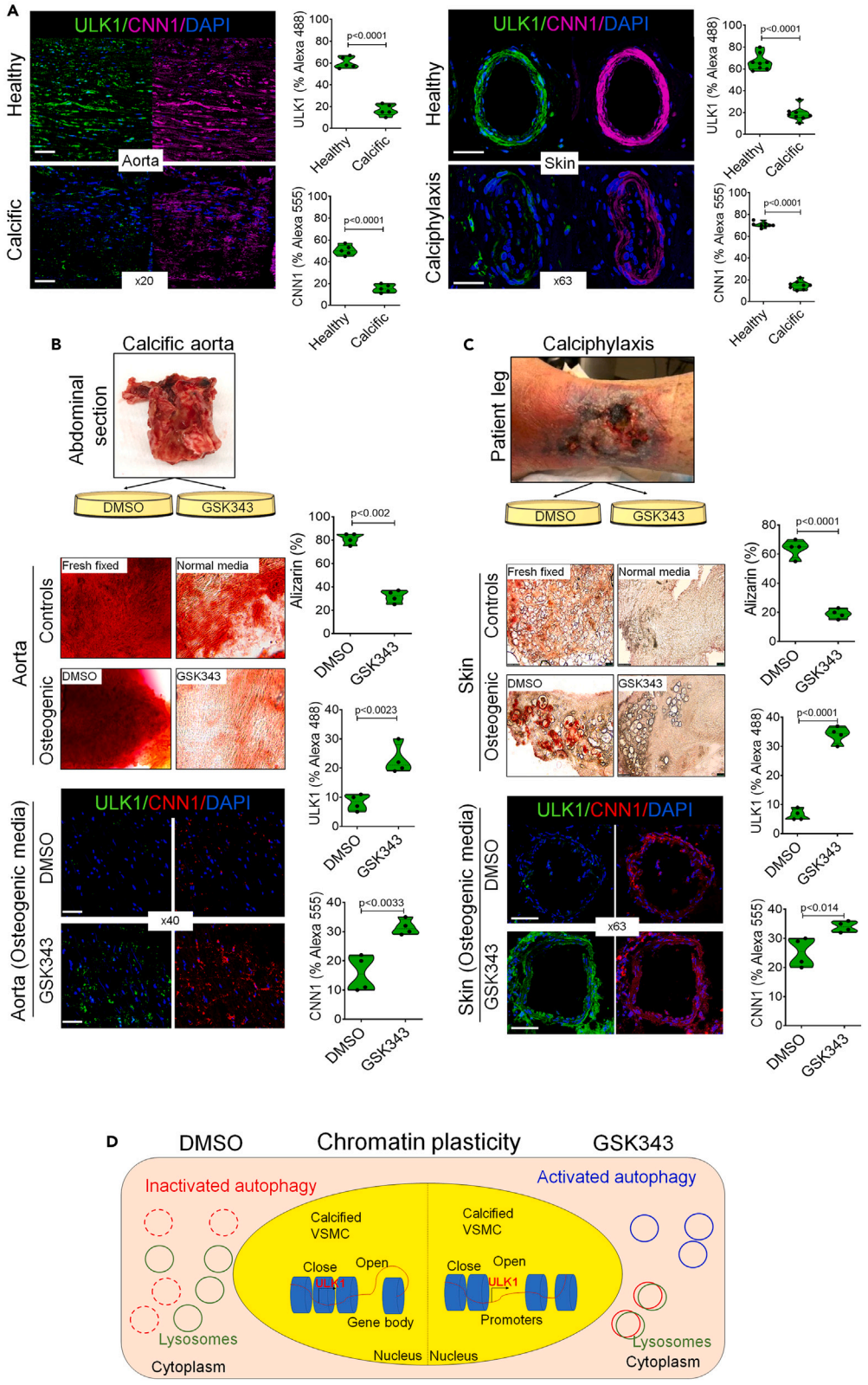
A
ULK1/CNN1/DAPI
Healthy
Calcific
Aorta
x20
ULK1 (% Alexa 488)
CNN1 (% Alexa 555)
p<0.0001
Healthy
Calcific
Calciphylaxis
Skin
x63
B
Calcific aorta
Abdominal section
DMSO
GSK343
Aorta
Controls
Osteogenic
Fresh fixed
Normal media
Alizarin (%)
p<0.002
p<0.0023
p<0.0033
Aorta (Osteogenic media)
x40
C
Calciphylaxis
Patient leg
Skin
p<0.0001
p<0.014
Skin (Osteogenic media)
D
DMSO
Chromatin plasticity
GSK343
Inactivated autophagy
Activated autophagy
Calcified VSMC
Close
Open
ULK1
Gene body
Promoters
Nucleus
Lysosomes
Cytoplasm

Figure 3. Therapeutic activation of autophagy by GSK343 inhibits calcification in *ex vivo* calcification

(A) Immunofluorescence staining showing reduced ULK1 (green) and CNN1 (magenta) levels in fresh-fixed tissue of human calcified aortas (left panel) and dermal biopsies from calciphylaxis (right panel) compared with healthy controls.

(B) *Ex vivo* calcification assays were performed with fresh surgical biopsies from patients with either aortic calcification (left panel) or (C) calciphylaxis (right panel). Alizarin red staining shows the calcification levels of surgical biopsies in normal or osteogenic media treated for 21 days with DMSO or GSK343 (20 μM). Treatment with GSK343 inhibited the *ex vivo* calcification of aortic and calciphylaxis tissues (middle panels) and was associated with increased ULK1 and CNN1 expression (lower panel).

(D) In our summative model of autophagy in VSMC calcification, defects in the autophagy initiation machinery at the transcriptional level impair autophagy flux and exacerbate calcification of VSMCs. GSK343 pharmacologically activates autophagy by relaxing chromatin and restoring expression of autophagy initiation genes (e.g., ULK1, BECN1, ATG13) to favor the formation of autolysosomes, which associates with inhibition of VSMC calcification. p values determined as compared with the corresponding control, by one-sample t test. Scale bars = 50 um.

Therapeutic and genetic activation of autophagy initiation inhibits vascular calcification in two different mouse models

The LC3 double reporter (RFP-GFP-LC3) mouse[25] (Figure 4A) enables quantification of autophagy flux *in vivo*. GFP emits strong fluorescence at a neutral pH, but the fluorescence is quenched in acidic conditions, such as in autolysosomes. RFP fluorescence, on the other hand, is stable under acidic conditions. Therefore, autophagosomes at a neutral pH will emit both a GFP and RFP signal, thus appearing yellow, whereas autolysosomes (a sign of productive autophagy flux) will emit just an RFP signal. We therefore used the RFP-GFP-LC3 mice to characterize autophagy flux in matrix-Gla-protein-deficient ($Mgp^{-/-}$) mice, a model of spontaneous large vessel calcification.[2] Microscopy analysis of the RFP-GFP-LC3 in the aortas of the $Mgp^{-/-}$ mice showed accumulation of yellow puncta (autophagosomes), whereas wild-type aortas showed increased numbers of red puncta (autolysosomes), suggesting that impairment of autophagy flux with calcification also occurs *in vivo* (Figure 4B). Moreover, mRNA levels of the autophagy initiation genes ULK1 and ULK2 were significantly down-regulated in the $Mgp^{-/-}$ aortas compared with wild-type aortas, in association with increased Runx2 mRNA levels, pointing toward a defect of the initiation step of autophagy (Figure 4C).

We next sought to evaluate the effect of pharmacologic agonism (GSK343) or genetic activation (Bcln1-F121A hyperactivating mutant knock-in)[26] of autophagy in two different *in vivo* models, one of diffuse arterial calcification ($Mgp^{-/-}$) and the second of dermal arterial calcification ($Abcc6^{-/-}$).[27] In Figure 5A (left panel), compared with wild-type mice, untreated $Mgp^{-/-}$ mice show an accumulation of LC3 (high RFP-GFP), suggesting impaired autophagy flux. However, $Mgp^{-/-}$ mice treated with GSK343 exhibited a dose-dependent decrease in LC3 signal, suggesting restoration of autophagy flux with appropriate recycling of the autolysosome. Similarly, genetic augmentation of autophagy initiation with Bcln1-F121A knock-in also decreased LC3 signal in $Mgp^{-/-}$ aortas, suggesting restoration of autophagy flux (Figure 5A, right panel). Due to severe aortic calcification, $Mgp^{-/-}$ mice typically die by ~5–6 weeks of age from aortic rupture.[3,28] However, activation of autophagy in $Mgp^{-/-}$ mice treated with GSK343 (median survival 69 days) or with Bcln1-F121A knock-in (median survival 68 days for homozygous knock-in mice) improved survival compared with control $Mgp^{-/-}$ mice with a median survival of 39.5 days (Log rank $p < 0.0001$ for each pairwise comparison with control $Mgp^{-/-}$, Figure 5B). Improved survival with increased autophagy was associated with reduced calcium deposition in the aortas of 35-day-old mice as assessed by alizarin red staining, improvement in aortic wall integrity as observed by elastin VVG stain, and increased expression of VSMC contractile protein CNN1 by immunofluorescence (Figure 5C). A similar strategy to augment autophagy initiation was employed with $Abcc6^{-/-}$ mice, a model of spontaneous dermal and arterial calcification bearing a deficiency in the gene that is mutated in pseudoxanthoma elasticum. In Figure 5D, compared with wild-type mice, the skin of $Abcc6^{-/-}$ mice show an accumulation of LC3 (high RFP-GFP), suggesting impaired autophagy flux. However, $Abcc6^{-/-}$ mice treated with GSK343 exhibited a decrease in LC3 signal, suggesting improved autophagy flux with appropriate recycling of the autolysosome. Similarly, genetic augmentation of autophagy initiation with hyperactive Becn1-F121A also decreased LC3 signal in $Abcc6^{-/-}$ mice, suggesting restoration of autophagy flux. Furthermore, activation of autophagy with GSK343 or with Bcln1-F121A in $Abcc6^{-/-}$ mice reduced dermal calcification as assessed by alizarin red stain (Figure 5E, lower panel). Interestingly the subcutaneous vascular anomalies characterized by reduced microvascular density in Abcc6-deficiency[29] also improved in either pharmacologic or genetic activation of autophagy (Figure 5E upper panel). Overall, these results provide evidence for impaired autophagy flux in two *in vivo* models of vascular calcification and highlight the potential therapeutic benefits of autophagy activation with GSK343 in treating vascular calcification.

DISCUSSION

Vascular calcification is a tightly regulated, cell-mediated process that leads to the deposition and accumulation of calcium phosphate in the extracellular matrix of vessel walls by secreted matrix vesicles. Autophagy is a fundamental cellular process also involving intracellular vesicles by which the cell degrades and recycles its own damaged or unnecessary components via autophagosome formation and subsequent lysosomal fusion. The interplay between autophagy and vascular calcification is complex, and prior studies have shown an important role for autophagy in VSMC calcification albeit with mixed and differing results at times.[30–32] In this study, we performed a comprehensive transcriptomic assessment of human VSMCs under calcifying conditions and found that genes specifically involved in the initiation of autophagy (i.e., ULK1, ULK2, ATG13) exhibit marked downregulated expression that was associated with reduced promoter accessibility on ATAC-Seq. Pharmacologic inhibition of ULK1 worsened calcification of VSMCs and *ex vivo* aortic explants, whereas pharmacologic activation of autophagy with GSK343 and rapamycin prevented the osteogenic switch and calcification of VSMCs and rescued the expression of autophagy initiation genes. In *in vivo* studies, impaired autophagy flux was a hallmark of large- and small-vessel calcification in two mouse models (MGP deficiency and pseudoxanthoma elasticum), and either pharmacologic or genetic restoration of autophagy improved survival and reduced vascular

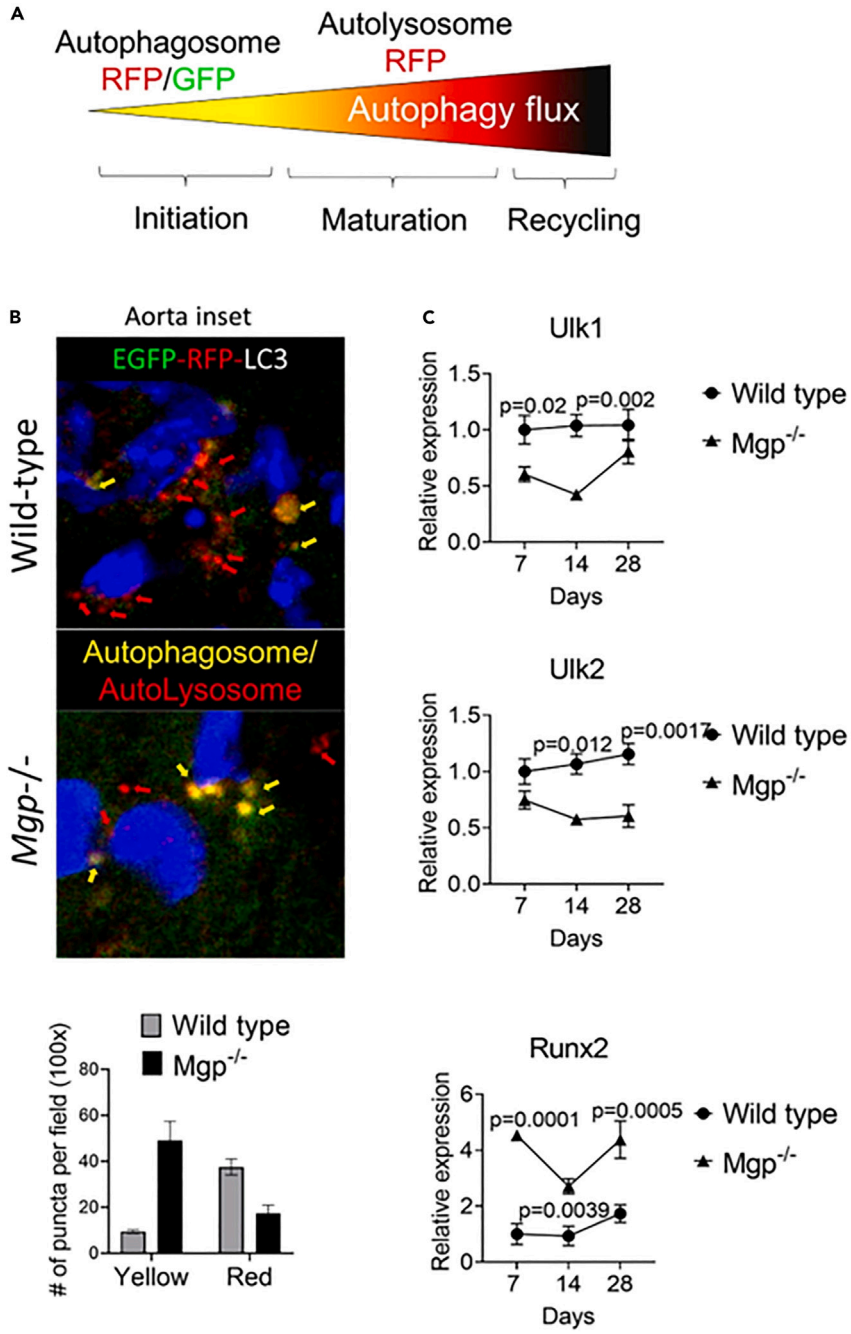

Figure 4. Impaired autophagy flux with deficiency in the expression of autophagy initiation genes characterize the aortas of a mouse model of vascular calcification

(A) Schematic representation of the *in vivo* model of assessing autophagy flux using the LC3 double reporter (RFP-GFP-LC3) mouse. Yellow puncta represent autophagosomes, whereas red puncta represent autolysosomes (autophagosome-lysosome fusion).

(B) Microscopy analysis of autophagosomes (yellow puncta) and autolysosomes (red puncta) in wild-type or *Mgp*$^{-/-}$ aortas expressing RFP-GFP-LC3. Puncta quantification show increased autophagosomes (yellow puncta) in *Mgp*$^{-/-}$, indicating lack of autolysosome formation due to impaired autophagy flux.

(C) mRNA levels of autophagy initiation genes from *Mgp*$^{-/-}$ and wild-type aortas. p values determined as compared with the corresponding control, by one-sample t test. Scale bars = 50 um.

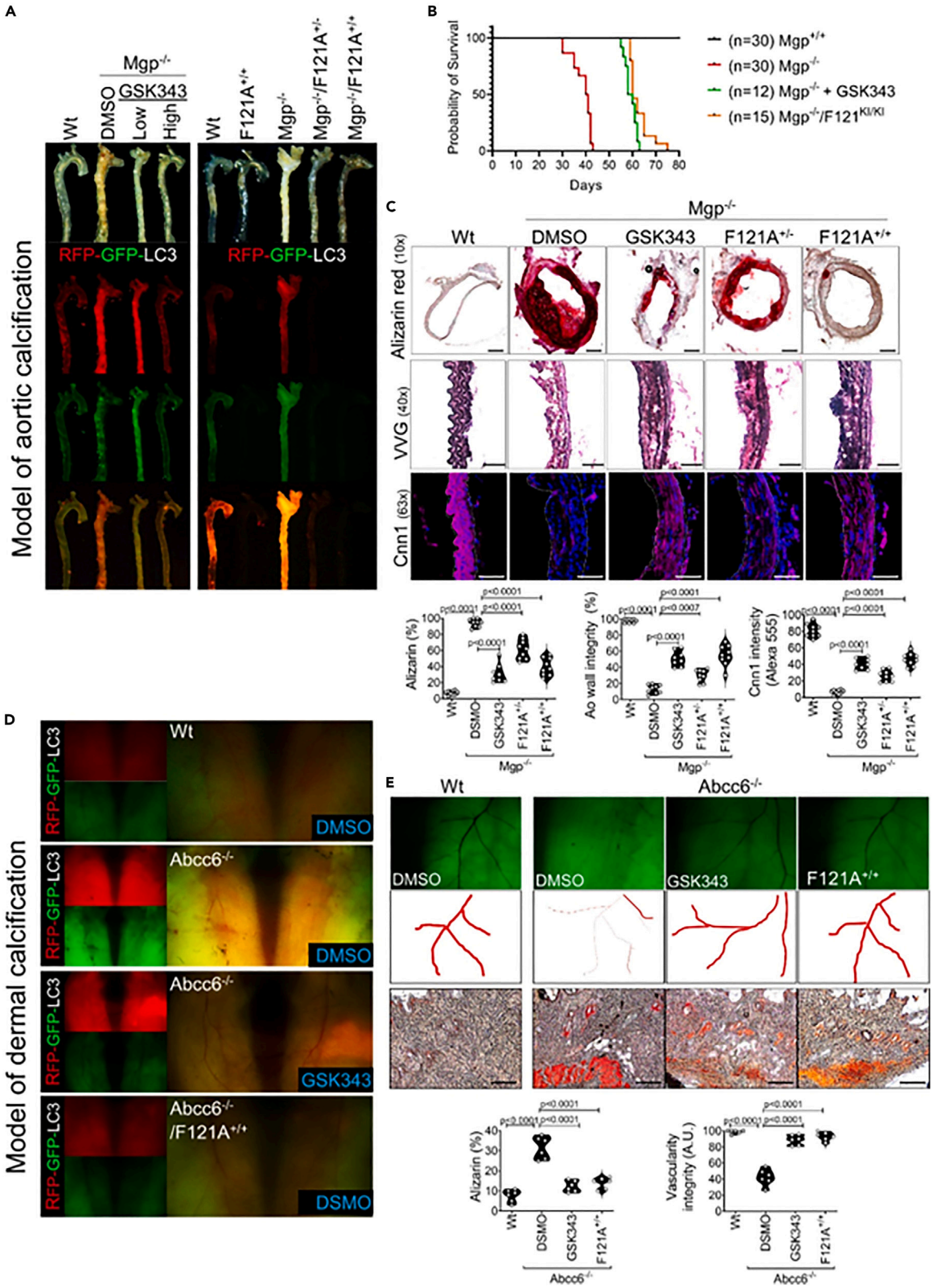
A
Model of aortic calcification
Wt
DMSO
Mgp-/-
GSK343
Low
High
F121A+/+
Mgp-/-
Mgp-/-/F121A+/-
Mgp-/-/F121A+/+
RFP-GFP-LC3
B
Probability of Survival
Days
(n=30) Mgp+/+
(n=30) Mgp-/-
(n=12) Mgp-/- + GSK343
(n=15) Mgp-/-/F121KI/KI
C
Mgp-/-
Wt
DMSO
GSK343
F121A+/-
F121A+/+
Alizarin red (10x)
VVG (40x)
Cnn1 (63x)
Alizarin (%)
Ao wall integrity (%)
Cnn1 intensity (Alexa 555)
D
Model of dermal calcification
Wt
Abcc6-/-
DMSO
GSK343
Abcc6-/-/F121A+/+
E
Wt
Abcc6-/-
Alizarin (%)
Vascularity integrity (A.U.)

Figure 5. Therapeutic and genetic activation of autophagy initiation inhibits vascular calcification in two different mouse models

(A) Pharmacologic (GSK343, low dose: 100μM and high dose: 400μM, see STAR Methods) and genetic (Bcn1^{F121A} mouse) activation of autophagy initiation in an animal model of aortic calcification (*Mgp*$^{-/-}$ mouse) shows restoration of autophagy flux as assessed by the RFP-GFP-LC3 reporter.

(B) Either pharmacologic activation of autophagy with GSK343 treatment or genetic activation of autophagy with the Bcn1^{F121A} mouse improves survival in *Mgp*$^{-/-}$ mice. Kaplan-Meier survival curves are depicted. Log rank $p < 0.0001$ for *Mgp*$^{-/-}$ vs. *Mgp*$^{-/-}$ treated with GSK343. Log rank $p < 0.0001$ for *Mgp*$^{-/-}$ vs. *Mgp*$^{-/-}$/F121$^{KI/KI}$ mice.

(C) Representative micrographs of alizarin red-, VVG-, and CNN1-stained sections of aortas are depicted.

(D) Pharmacologic (GSK343, high dose, see STAR Methods) and genetic (Bcn1^{F121A} mouse) activation of autophagy initiation in the animal model of dermal calcification (*Abcc6*$^{-/-}$ mouse) shows restoration of autophagy flux as assessed by the RFP-GFP-LC3 reporter.

(E) Representative micrographs (GFP channel) of abdominal skin small arteries (top panel), with a schematic representation in the middle panel showing normal skin microvascularity in *Abcc6*$^{-/-}$ mice with autophagy activation compared with control *Abcc6*$^{-/-}$ mice. Lower panel shows alizarin red staining of histologic skin sections with reduced calcification in *Abcc6*$^{-/-}$ mice with autophagy activation induced either pharmacologically with GSK343 or genetically (Becn1^{F121A}). Significance was calculated using 1-way ANOVA with a Tukey's multi-comparisons test. Scale bars = 50 um.

calcification. Moreover, we report that SNPs in multiple genes critical for autophagy initiation as well as mRNA expression of autophagy initiation genes are tightly linked to calcification-related diseases in humans, including ischemic coronary artery disease and peripheral arterial disease. Altogether, these results highlight an essential role for autophagy in vascular calcification with strong associations to human vascular disease.

The balance between calcifying matrix vesicle release and autophagy in the context of VSMC calcification was first demonstrated by Dai et al. who showed that phosphate-induced autophagy in VSMCs was dependent on the production of reactive oxygen species and protected the cells from calcifying.[33] Pharmacologic inhibition of autophagy *in vitro* with 3-methyladenine, an inhibitor of PI-3 kinase that regulates mTOR activity, increased VSMC calcification. This study showed the importance of autophagy in regulating VSMC calcification *in vitro*. Our results extend these findings by highlighting the specific dysregulation of genes important for autophagy initiation in the calcification of VSMCs. Furthermore, our study demonstrated abnormal autophagy flux *in vivo* using RFP-GFP-LC3 reporter mice in the context of vascular calcification. Autophagy activation is protective against uremic medial calcification as well as atherosclerotic intimal calcification.[30,34] Our results demonstrate an essential role for autophagy in both the large vessel medial calcification associated with MGP deficiency and the small vessel calcification of pseudoxanthoma elasticum, underscoring an important overall role for autophagy in vascular homeostasis.

VSMCs are the principal cellular components of arterial vessels and play a critical role in regulating vascular tone and blood flow and maintaining vascular homeostasis in vascular injury. A hallmark of VSMCs is their phenotypic heterogeneity, as they can transition from a quiescent, contractile phenotype to a synthetic, osteogenic phenotype expressing markers of bone. These osteogenic VSMCs exhibit reduced contractile protein machinery (i.e., calponin, SM22α, SM actin) and increased migration, proliferation, and matrix vesicle secretion and are associated with diseases such as atherosclerosis, diabetes, hypertension, and chronic kidney disease.[35] We show evidence that intact autophagy is required to maintain a normal contractile VSMC phenotype and that pharmacologic activation of autophagy can maintain the contractile state of VSMCs even under calcifying conditions. Interestingly, the matrix vesicles that are secreted by osteogenic VSMCs are not only enriched in calcium, phosphate, and phosphate-regulating enzymes such as alkaline phosphatase but also express autophagic proteins including LAMP1 and LAMP2.[36] Indeed, autophagy involves both the conventional auto-digestive processes as well as non-degradative, secretory processes (termed secretory autophagy) that help to excrete particulate substrates.[37] Although there is some overlap in the regulatory proteins involved, secretory autophagy generally has different mediators than conventional auto-digestive autophagy. Further investigation is needed to specifically determine if the balance between auto-digestive and secretory autophagy regulates vascular calcification.

Calcification of VSMCs has been previously shown to depend on the methylation state of the SM22α promoter, and inhibition of DNA methyltransferase activity inhibited *in vitro* calcification.[38] The state of chromatin defined by the packaging of DNA with histone and nonhistone proteins into areas of relative accessibility and repression profoundly affects gene expression and regulates cellular identity.[39] Autophagy, in response to environmental cues and stimuli, has been implicated in regulating the differentiation of numerous cell types and plays an important role in angiogenesis and vascular homeostasis.[14,15] Our results provide evidence that exposure of VSMCs to calcifying conditions impairs autophagy at least in part through large-scale adjustments in chromatin state and that activation of autophagy inhibits the osteogenic phenotype switch of VSMCs. Prior work identified important roles for epigenetic regulators in vascular calcification including histone deacetylases and methyltransferases.[6,40,41] A number of studies have demonstrated that histone methyltransferases play an important role in autophagy. EZH2 is the active subunit of the polycomb repressive complex 2 (PRC2) and functions as a histone methyltransferase that di- and tri-methylates H3 at lys27 (H3K27) to suppress autophagy-related gene transcription.[6,42] Here, we demonstrated that EZH2 inhibition with GSK343 increases chromatin accessibility at the sites of autophagy initiation genes in VSMCs and that this was associated with an inhibition of osteogenic phenotype switch and calcification. Moreover, GSK343 inhibited vascular calcification and improved survival outcomes *in vivo*.

Studies have shown that impaired autophagy is associated with several pathological conditions including cancer, neurodegenerative disease, cardiovascular disease, immune disorders, and metabolic disorders such as diabetes and obesity. The link between impaired autophagy and these diseases is thought to be due to the inability of cells to properly remove damaged or abnormal components, leading to the accumulation of harmful molecules and organelles, chronic inflammation, and cellular stress. Additionally, aging has been associated with impaired autophagy. Autophagy declines as we age due to many factors,[43] and the accumulation of damaged cellular components is a key contributor to aging-related diseases. Although we believe that our findings are relevant for chronic calcification disorders, a limitation

in this study is that our *in vitro* and *in vivo* models represent aggressive forms of acute calcification. Therefore, future studies directed at studying the role of impaired autophagy in aging-related chronic cardiovascular calcification disorders may identify novel targets of therapy for these more common diseases.

In conclusion, impaired autophagy is a serious condition that can contribute to vascular calcification and other cardiovascular diseases and metabolic disorders. To our knowledge, our data provide the first association of impaired autophagy in calciphylaxis and pseudoxanthoma elasticum, two highly morbid conditions that have no targeted therapy. Similar to our findings, autophagy activation is protective against uremic medial calcification as well as atherosclerotic intimal calcification, underscoring an important role for autophagy in vascular homeostasis. Our results specifically implicate impaired autophagy initiation in VSMC-mediated calcification. Altogether, these findings advance our mechanistic understanding of vascular calcification by specifically implicating impairment of the autophagy pathway and provide important insights for a broad range of cardiovascular diseases involving VSMC phenotype switch. This proof-of-concept preclinical study suggests that pharmacologic enhancers of autophagy could have a role in the future medical treatment of vascular calcific disorders.

Limitations of the study

Although our findings are relevant to chronic and severe calcification, our study has a limitation in that our *in vitro* and *in vivo* models only represent aggressive calcification. Therefore, future studies employing chronic models of calcification will aid in evaluating whether the promotion of autophagy flux using GSK343 or gene therapy can facilitate the reversal of arterial calcification. In conclusion, our results suggest that impaired initiation of autophagy plays a role in vascular calcification. Currently, there is no targeted medical treatment for preventing vascular calcification. However, our proof-of-concept preclinical study proposes that pharmacological enhancers of autophagy may have a future role in the medical treatment of vascular calcific disorders.

STAR★METHODS

Detailed methods are provided in the online version of this paper and include the following:

- KEY RESOURCES TABLE
- RESOURCE AVAILABILITY
  - Lead contact
  - Materials availability
  - Data and code availability
- EXPERIMENTAL MODEL AND STUDY PARTICIPANT DETAILS
  - Animal models
  - *In vivo* GSK343 treatment
  - Histology
  - Blind test of aortic wall integrity
- METHODS DETAILS
  - Human aortic tissue and calciphylaxis tissue
  - Human coronary artery tissue procurement
  - Coronary artery RNA extraction, QC, library construction and sequencing
  - Coronary artery RNA-seq processing and analysis
  - Coronary artery differential gene expression analysis
  - Aortic smooth muscle cell lines
  - *In vitro* model of VSMC calcification
  - Immunoblotting
  - RNA isolation and RNA-seq analysis
  - ATAC-seq
  - FISH and immunofluorescence microscopy
  - *Ex vivo* models
  - Collagen gel contraction assay
  - Calcium assay
- QUANTIFICATION AND STATISTICAL ANALYSIS
  - Summary-based Mendelian randomization analysis
  - Activity-by-contact (ABC) enhancer-gene analysis
  - Statistics

SUPPLEMENTAL INFORMATION

Supplemental information can be found online at https://doi.org/10.1016/j.isci.2023.108360.

ACKNOWLEDGMENTS

Dr. Malhotra was supported by the National Heart, Lung, and Blood Institute (R01HL142809 and R01HL162928), the American Heart Association (22TPA969625), and the Wild Family Foundation. Dr. Lino Cardenas was supported by NIH K01HL164687. The content of this paper is solely the responsibility of the authors and does not necessarily represent official views of the NIH.

AUTHOR CONTRIBUTIONS

C.L.L.C., R.M., Z.D., and C.L.M. conceptualized and designed the study. W.J., K.S., K.O., R.L., F.C., S.B., C.B., Z.S., and C.N. performed the experiments, acquired, and interpreted the data. E.L.C. and S.N. provided biopsy samples. L.K., K.R., M.E.L., P.M., P.T.E., A.L.J., S.L., F.I., and D.B.B. provided clinical input and critical interpretation. All authors provided revisions for the manuscript. Authorship order among the co-first authors was based on relative contributions of co-author input to the final manuscript. All authors reviewed and approved the final version of the manuscript.

DECLARATION OF INTERESTS

Dr. Lino Cardenas receives research funding from Angea Biotherapeutics. Dr. Malhotra receives research funding from Angea Biotherapeutics and Amgen and serves as a consultant for Myokardia/BMS, Renovacor, Epizon Pharma, and Third Pole. Dr. Malhotra is a co-inventor for a patent on pharmacologic BMP inhibitors (along with Mass General Brigham) for which he receives royalties. Dr. Malhotra also receives royalties from UpToDate for scientific content authorship.

INCLUSION AND DIVERSITY

We support inclusive, diverse, and equitable conduct of research.

Received: June 26, 2023
Revised: August 31, 2023
Accepted: October 25, 2023
Published: October 29, 2023

REFERENCES

1. Chen, T., and Dent, S.Y. (2014). Chromatin modifiers and remodellers: regulators of cellular differentiation. Nat. Rev. Genet. *15*, 93–106. https://doi.org/10.1038/nrg3607.
2. Luo, G., Ducy, P., McKee, M.D., Pinero, G.J., Loyer, E., Behringer, R.R., and Karsenty, G. (1997). Spontaneous calcification of arteries and cartilage in mice lacking matrix GLA protein. Nature *386*, 78–81. https://doi.org/10.1038/386078a0.
3. Malhotra, R., Burke, M.F., Martyn, T., Shakartzi, H.R., Thayer, T.E., O'Rourke, C., Li, P., Derwall, M., Spagnolli, E., Kolodziej, S.A., et al. (2015). Inhibition of bone morphogenetic protein signal transduction prevents the medial vascular calcification associated with matrix Gla protein deficiency. PLoS One *10*, e0117098. https://doi.org/10.1371/journal.pone.0117098.
4. Bostrom, K., Watson, K.E., Horn, S., Wortham, C., Herman, I.M., and Demer, L.L. (1993). Bone morphogenetic protein expression in human atherosclerotic lesions. J. Clin. Invest. *91*, 1800–1809. https://doi.org/10.1172/JCI116391.
5. Byon, C.H., Javed, A., Dai, Q., Kappes, J.C., Clemens, T.L., Darley-Usmar, V.M., McDonald, J.M., and Chen, Y. (2008). Oxidative stress induces vascular calcification through modulation of the osteogenic transcription factor Runx2 by AKT signaling. J. Biol. Chem. *283*, 15319–15327. https://doi.org/10.1074/jbc.M800021200.
6. Hou, Y.C., Lu, C.L., Yuan, T.H., Liao, M.T., Chao, C.T., and Lu, K.C. (2020). The Epigenetic Landscape of Vascular Calcification: An Integrative Perspective. Int. J. Mol. Sci. *21*, 980. https://doi.org/10.3390/ijms21030980.
7. Jin, H.Y., Weir-McCall, J.R., Leipsic, J.A., Son, J.W., Sellers, S.L., Shao, M., Blanke, P., Ahmadi, A., Hadamitzky, M., Kim, Y.J., et al. (2021). The Relationship Between Coronary Calcification and the Natural History of Coronary Artery Disease. JACC Cardiovasc Imaging *14*, 233–242. https://doi.org/10.1016/j.jcmg.2020.08.036.
8. Klarin, D., Lynch, J., Aragam, K., Chaffin, M., Assimes, T.L., Huang, J., Lee, K.M., Shao, Q., Huffman, J.E., Natarajan, P., et al. (2019). Genome-wide association study of peripheral artery disease in the Million Veteran Program. Nat Med *25*, 1274–1279. https://doi.org/10.1038/s41591-019-0492-5.
9. Jiang, P., and Mizushima, N. (2014). Autophagy and human diseases. Cell Res. *24*, 69–79. https://doi.org/10.1038/cr.2013.161.
10. Levine, B., and Kroemer, G. (2019). Biological Functions of Autophagy Genes: A Disease Perspective. Cell *176*, 11–42. https://doi.org/10.1016/j.cell.2018.09.048.
11. Zhou, X., Xu, S.N., Yuan, S.T., Lei, X., Sun, X., Xing, L., Li, H.J., He, C.X., Qin, W., Zhao, D., et al. (2021). Multiple functions of autophagy in vascular calcification. Cell Biosci. *11*, 159. https://doi.org/10.1186/s13578-021-00639-9.
12. Mizushima, N. (2010). The role of the Atg1/ULK1 complex in autophagy regulation. Curr. Opin. Cell Biol. *22*, 132–139. https://doi.org/10.1016/j.ceb.2009.12.004.
13. Mizushima, N., and Levine, B. (2010). Autophagy in mammalian development and differentiation. Nat. Cell Biol. *12*, 823–830. https://doi.org/10.1038/ncb0910-823.
14. Perrotta, C., Cattaneo, M.G., Molteni, R., and De Palma, C. (2020). Autophagy in the Regulation of Tissue Differentiation and Homeostasis. Front. Cell Dev. Biol. *8*, 602901. https://doi.org/10.3389/fcell.2020.602901.
15. Zhao, Y.G., Codogno, P., and Zhang, H. (2021). Machinery, regulation and pathophysiological implications of autophagosome maturation. Nat. Rev. Mol. Cell Biol. *22*, 733–750. https://doi.org/10.1038/s41580-021-00392-4.
16. Abdellatif, M., Sedej, S., Carmona-Gutierrez, D., Madeo, F., and Kroemer, G. (2018). Autophagy in Cardiovascular Aging. Circ. Res. *123*, 803–824. https://doi.org/10.1161/CIRCRESAHA.118.312208.
17. Lin, L., Zhang, M.X., Zhang, L., Zhang, D., Li, C., and Li, Y.L. (2021). Autophagy, Pyroptosis, and Ferroptosis: New Regulatory Mechanisms for Atherosclerosis. Front. Cell Dev. Biol. *9*, 809955. https://doi.org/10.3389/fcell.2021.809955.
18. Egan, D.F., Chun, M.G., Vamos, M., Zou, H., Rong, J., Miller, C.J., Lou, H.J., Raveendra-Panickar, D., Yang, C.C., Sheffler, D.J., et al. (2015). Small Molecule Inhibition of the Autophagy Kinase ULK1 and Identification of ULK1 Substrates. Mol Cell *59*, 285–297. https://doi.org/10.1016/j.molcel.2015.05.031.
19. Nigwekar, S.U., Bloch, D.B., Nazarian, R.M., Vermeer, C., Booth, S.L., Xu, D., Thadhani, R.I., and Malhotra, R. (2017). Vitamin K-Dependent Carboxylation of Matrix Gla Protein Influences the Risk of Calciphylaxis. J. Am. Soc. Nephrol. *28*, 1717–1722. https://doi.org/10.1681/ASN.2016060651.

20. Franceschini, N., Giambartolomei, C., de Vries, P.S., Finan, C., Bis, J.C., Huntley, R.P., Lovering, R.C., Tajuddin, S.M., Winkler, T.W., Graff, M., et al. (2018). GWAS and colocalization analyses implicate carotid intima-media thickness and carotid plaque loci in cardiovascular outcomes. Nat. Commun. *9*, 5141. https://doi.org/10.1038/s41467-018-07340-5.
21. Kim, K.H., and Roberts, C.W. (2016). Targeting EZH2 in cancer. Nat Med *22*, 128–134. https://doi.org/10.1038/nm.4036.
22. Xu, H., Zhang, L., Qian, X., Zhou, X., Yan, Y., Zhou, J., Ge, W., Albahde, M., and Wang, W. (2019). GSK343 induces autophagy and downregulates the AKT/mTOR signaling pathway in pancreatic cancer cells. Exp. Ther. Med. *18*, 2608–2616. https://doi.org/10.3892/etm.2019.7845.
23. Lamming, D.W. (2016). Inhibition of the Mechanistic Target of Rapamycin (mTOR)-Rapamycin and Beyond. Cold Spring Harb Perspect Med *6*, a025924. https://doi.org/10.1101/cshperspect.a025924.
24. Xu, W., Wen, Y., Liang, Y., Xu, Q., Wang, X., Jin, W., and Chen, X. (2021). A plate-based single-cell ATAC-seq workflow for fast and robust profiling of chromatin accessibility. Nat. Protoc. *16*, 4084–4107. https://doi.org/10.1038/s41596-021-00583-5.
25. Li, L., Wang, Z.V., Hill, J.A., and Lin, F. (2014). New autophagy reporter mice reveal dynamics of proximal tubular autophagy. J. Am. Soc. Nephrol. *25*, 305–315. https://doi.org/10.1681/ASN.2013040374.
26. Rocchi, A., Yamamoto, S., Ting, T., Fan, Y., Sadleir, K., Wang, Y., Zhang, W., Huang, S., Levine, B., Vassar, R., and He, C. (2017). A Becn1 mutation mediates hyperactive autophagic sequestration of amyloid oligomers and improved cognition in Alzheimer's disease. PLoS Genet. *13*, e1006962. https://doi.org/10.1371/journal.pgen.1006962.
27. Klement, J.F., Matsuzaki, Y., Jiang, Q.J., Terlizzi, J., Choi, H.Y., Fujimoto, N., Li, K., Pulkkinen, L., Birk, D.E., Sundberg, J.P., and Uitto, J. (2005). Targeted ablation of the abcc6 gene results in ectopic mineralization of connective tissues. Mol. Cell Biol. *25*, 8299–8310. https://doi.org/10.1128/MCB.25.18.8299-8310.2005.
28. Malhotra, R., Mauer, A.C., Lino Cardenas, C.L., Guo, X., Yao, J., Zhang, X., Wunderer, F., Smith, A.V., Wong, Q., Pechlivanis, S., et al. (2019). HDAC9 is implicated in atherosclerotic aortic calcification and affects vascular smooth muscle cell phenotype. Nat. Genet. *51*, 1580–1587. https://doi.org/10.1038/s41588-019-0514-8.
29. Stumpf, M.J., Mahn, T., Steinmetz, M., Fimmers, R., Pizarro, C., Nickenig, G., Skowasch, D., Schahab, N., and Schaefer, C.A. (2020). Pseudoxanthoma elasticum - also a microvascular disease. Vasa *49*, 57–62. https://doi.org/10.1024/0301-1526/a000811.
30. Frauscher, B., Kirsch, A.H., Schabhüttl, C., Schweighofer, K., Kétszeri, M., Pollheimer, M., Dragun, D., Schröder, K., Rosenkranz, A.R., Eller, K., and Eller, P. (2018). Autophagy Protects From Uremic Vascular Media Calcification. Front. Immunol. *9*, 1866. https://doi.org/10.3389/fimmu.2018.01866.
31. Heath, J.M., Sun, Y., Yuan, K., Bradley, W.E., Litovsky, S., Dell'Italia, L.J., Chatham, J.C., Wu, H., and Chen, Y. (2014). Activation of AKT by O-linked N-acetylglucosamine induces vascular calcification in diabetes mellitus. Circ. Res. *114*, 1094–1102. https://doi.org/10.1161/circresaha.114.302968.
32. Salabei, J.K., Cummins, T.D., Singh, M., Jones, S.P., Bhatnagar, A., and Hill, B.G. (2013). PDGF-mediated autophagy regulates vascular smooth muscle cell phenotype and resistance to oxidative stress. Biochem. J. *451*, 375–388. https://doi.org/10.1042/bj20121344.
33. Dai, X.Y., Zhao, M.M., Cai, Y., Guan, Q.C., Zhao, Y., Guan, Y., Kong, W., Zhu, W.G., Xu, M.J., and Wang, X. (2013). Phosphate-induced autophagy counteracts vascular calcification by reducing matrix vesicle release. Kidney Int. *83*, 1042–1051. https://doi.org/10.1038/ki.2012.482.
34. Poznyak, A.V., Nikiforov, N.G., Wu, W.K., Kirichenko, T.V., and Orekhov, A.N. (2021). Autophagy and Mitophagy as Essential Components of Atherosclerosis. Cells *10*, 443. https://doi.org/10.3390/cells10020443.
35. Zhang, F., Guo, X., Xia, Y., and Mao, L. (2021). An update on the phenotypic switching of vascular smooth muscle cells in the pathogenesis of atherosclerosis. Cell. Mol. Life Sci. *79*, 6. https://doi.org/10.1007/s00018-021-04079-z.
36. Phadwal, K., Feng, D., Zhu, D., and MacRae, V.E. (2020). Autophagy as a novel therapeutic target in vascular calcification. Pharmacol. Ther. *206*, 107430. https://doi.org/10.1016/j.pharmthera.2019.107430.
37. Gonzalez, C.D., Resnik, R., and Vaccaro, M.I. (2020). Secretory Autophagy and Its Relevance in Metabolic and Degenerative Disease. Front. Endocrinol. *11*, 266. https://doi.org/10.3389/fendo.2020.00266.
38. Montes de Oca, A., Madueño, J.A., Martinez-Moreno, J.M., Guerrero, F., Muñoz-Castañeda, J., Rodriguez-Ortiz, M.E., Mendoza, F.J., Almaden, Y., Lopez, I., Rodriguez, M., and Aguilera-Tejero, E. (2010). High-phosphate-induced calcification is related to SM22α promoter methylation in vascular smooth muscle cells. J. Bone Miner. Res. *25*, 1996–2005. https://doi.org/10.1002/jbmr.93.
39. Shanahan, C.M., Cary, N.R., Metcalfe, J.C., and Weissberg, P.L. (1994). High expression of genes for calcification-regulating proteins in human atherosclerotic plaques. J. Clin. Invest. *93*, 2393–2402. https://doi.org/10.1172/JCI117246.
40. Lin, B., Srikanth, P., Castle, A.C., Nigwekar, S., Malhotra, R., Galloway, J.L., Sykes, D.B., and Rajagopal, J. (2018). Modulating Cell Fate as a Therapeutic Strategy. Cell Stem Cell *23*, 329–341. https://doi.org/10.1016/j.stem.2018.05.009.
41. Shankman, L.S., Gomez, D., Cherepanova, O.A., Salmon, M., Alencar, G.F., Haskins, R.M., Swiatlowska, P., Newman, A.A., Greene, E.S., Straub, A.C., et al. (2016). Corrigendum: KLF4-dependent phenotypic modulation of smooth muscle cells has a key role in atherosclerotic plaque pathogenesis. Nat Med *22*, 217. https://doi.org/10.1038/nm0216-217a.
42. Wei, F.Z., Cao, Z., Wang, X., Wang, H., Cai, M.Y., Li, T., Hattori, N., Wang, D., Du, Y., Song, B., et al. (2015). Epigenetic regulation of autophagy by the methyltransferase EZH2 through an MTOR-dependent pathway. Autophagy *11*, 2309–2322. https://doi.org/10.1080/15548627.2015.1117734.
43. Aman, Y., Schmauck-Medina, T., Hansen, M., Morimoto, R.I., Simon, A.K., Bjedov, I., Palikaras, K., Simonsen, A., Johansen, T., Tavernarakis, N., et al. (2021). Autophagy in healthy aging and disease. Nat Aging *1*, 634–650. https://doi.org/10.1038/s43587-021-00098-4.
44. Zhu, Z., Zhang, F., Hu, H., Bakshi, A., Robinson, M.R., Powell, J.E., Montgomery, G.W., Goddard, M.E., Wray, N.R., Visscher, P.M., and Yang, J. (2016). Integration of summary data from GWAS and eQTL studies predicts complex trait gene targets. Nat. Genet. *48*, 481–487. https://doi.org/10.1038/ng.3538.

STAR★METHODS

KEY RESOURCES TABLE

REAGENT or RESOURCE	SOURCE	IDENTIFIER
Antibodies		
Anti-RUNX2 (F-2)	Santa Cruz Biotechnology	sc-390351
Anti-ULK1 (D8H5)	Cell signaling	8054S
Anti-ULK2 (2A12)	Santa Cruz Biotechnology	sc-293453
Anti-ATG13 (E1Y9V)	Cell signaling	13468S
Anti-P62 (D1Q5S)	Cell signaling	39749S
Anti-CNN1(EP798Y)	Abcam	ab46794
Anti-SM22a	Abcam	ab14106
Anti-b-Actin (13E5)	Cell signaling	4970S
Anti-GAPDH (14C10)	Cell signaling	2118L
Anti-LAMP1 (D2D11)	Cell signaling	9091S
Anti-LC3B (E5Q2K)	Cell signaling	83506S
Anti-VCL (7F9)	Santa Cruz Biotechnology	sc-73614
Biological samples		
Human aortic tissue		
Human calciphylaxis tissue		
Human coronary artery		
Chemicals, peptides, and recombinant proteins		
Hydroxychloroquine Sulfate	Sigma-Aldrich	5092720001
Rapamycin	Sigma-Aldrich	553210-1MG
Alizarin red staining	Sigma-Aldrich	TMS-008-C
GSK343	Sigma-Aldrich	SML0766-25MG
Dimethyl sulfoxide	Sigma-Aldrich	D2650-5X10ML
MMPsense 680 Fluorescent Probe	Perkinelmer	NEV10126
Osteosense 800 Fluorescent Probe	Perkinelmer	NEV11105
Critical commercial assays		
Cell Contraction assay	Cell Biolabs, INC	CBA-201
Calcium Colorimetric Assay	Sigma-Aldrich	MAK022-1KT
Deposited data		
RNA-seq	GSE225650	
Experimental models: Cell lines		
HAOSMC	Cell Applications, INC	354-05a
Experimental models: Organisms/strains		
Mgp -/-	generated by G. Karsenty and colleagues from the Department of Molecular and Human Genetics, Baylor College of Medicine, Texas, USA.	
Abcc6 -/-	kindly provided by Dr. Jouni J. Uitto and Ida J. Jacobs from the Thomas Jefferson University, Philadelphia, USA.	
B6.129(Cg)-Becn1tm1.1Hec/J	kindly provided by Dr. Beth Levine from UT Southwestern Medical Center, USA.	
C57BL/6-Tg (CAG-RFP/EGFP/Map1lc3b)1Hill/J	The Jackson laboratory	027139

(*Continued on next page*)

Continued

REAGENT or RESOURCE	SOURCE	IDENTIFIER
Oligonucleotides		
ULK1	GGCAAGTTCGAGTTCTCCCG	CGACCTCCAAATCGTGCTTCT
ULK2	TGGAGACCTCGCAGATTATTTGC	CTGTGCAGGATTCGCATGG
BCL1	GGTGCCTGCTATGACAAGG	GGCTCGGACACTTTCCTGAG
ATG2	AACTGCTGACGAATCCTCAGG	GGGGTTCCAGCTAGGTGAGA
ATG3	GACCCCGGTCCTCAAGGAA	TGTAGCCCATTGCCATGTTGG
ATG4	ATGGACGCAGCTACTCTGAC	TTTTCTACCCAGTATCCAAACGG
ATG5	AAAGATGTGCTTCGAGATGTGT	CACTTTGTCAGTTACCAACGTCA
ATG7	CAGTTTGCCCCTTTTAGTAGTGC	CCAGCCGATACTCGTTCAGC
ATG12	CTGCTGGCGACACCAAGAAA	CGTGTTCGCTCTACTGCCC
ATG13	TTGCTATAACTAGGGTGACACCA	CCCAACACGAACTGTCTGGA
ATG14	GCGCCAAATGCGTTCAGAG	AGTCGGCTTAACCTTTCCTTCT
LAMP1	TCTCAGTGAACTACGACACCA	AGTGTATGTCCTCTTCCAAAAGC
LAMP2	GAAAATGCCACTTGCCTTTATGC	AGGAAAAGCCAGGTCCGAAC
Ulk1	AAGTTCGAGTTCTCTCGCAAG	ACCTCCAGGTCGTGCTTCT
Ulk2	CCAGAAAACTGATTGGGAGGTG	AAGACAGAGTTGGGCAATTCC
Runx2	GACTGTGGTTACCGTCATGGC	ACTTGGTTTTTCATAACAGCGGA

RESOURCE AVAILABILITY

Lead contact

Further information and requests for resources and reagents should be directed to and will be fulfilled by the lead contact, Rajeev Malhotra (rmalhotra@mgh.harvard.edu).

Materials availability

This study did not generate any unique new reagent. All reagents used in this study are commercially available.

Data and code availability

All data reported in this paper will be shared by the lead contact upon request. No custom code, software, or algorithm central to supporting the main claims of the paper were generated in this manuscript.

EXPERIMENTAL MODEL AND STUDY PARTICIPANT DETAILS

Animal models

All mice were cared for under strict compliance with the Partners Institutional Animal Care and Use Committee (IACUC), regulated by the United States Public Health Service (USPHS) and the United States Department of Agriculture (USDA). All procedures followed ethical standards to prioritize animal welfare and minimize suffering. Animals were handled with care throughout the study. We used 45 mice for this study. The number of animals per group was determined based on a statistical power analysis, aiming to reduce the number to the minimum required for valid statistical analyses. Mice were housed in a controlled environment with a temperature of 21-25°C, humidity of 40-60%, and a 12-hour light/dark cycle. Animals had access to standard laboratory chow and water *ad libitum*. Experimental procedures involved tissue collection post-mortem. Personnel involved in the procedures were appropriately trained to ensure consistency.

At the conclusion of the study or upon reaching predefined humane endpoints, animals were euthanized using CO2 asphyxiation followed by exsanguination in accordance with ARRIVE guidelines. Data were analyzed using GraphPad as detailed in statistic section.

This study was carried out in strict accordance with the recommendations in the Guide for the Care and Use of Laboratory Animals of the National Institutes of Health. Housing and all procedures involving mice described in this study were specifically approved by the Institutional Animal Care and Use Committees of Massachusetts General Hospital (Subcommittee on Research Animal Care, protocol #2008N000169). *Mgp*$^{-/-}$ mice were generated by G. Karsenty and colleagues. The model of small vessel dermal calcification (Abcc6$^{-/-}$ mice) was kindly provided by Dr. Jouni J. Uitto and Ida J. Jacobs from the Thomas Jefferson University, Philadelphia, USA. The animal model of hyperactivated autophagy (B6.129(Cg)-Becn1tm1.1Hec/J) was kindly provided by Dr. Beth Levine from UT Southwestern Medical Center, USA. The animal model of autophagy maturation reporter (C57BL/6-Tg (CAG-RFP/EGFP/Map1lc3b)1Hill/J, Stock No: 027139) was purchased from Jackson

Laboratory. Animals were maintained on a standard diet. Survival studies were performed and the Kaplan-Meier statistic with log-rank testing was used to compare survival of mice.

This Method section adheres to ARRIVE guidelines (https://arriveguidelines.org/), providing a comprehensive and clear description of the experimental procedures, ethical considerations, and statistical methods employed in our mouse study.

In vivo GSK343 treatment

20 mg/kg/day of GSK343 was administered via IP injection from P5 to P22 days of age. Then weaned mice received a low dose at 100uM or a higher dose at 400uM of GSK343 orally via water bottle administration. The treatment solution was replaced with fresh drug every 48 hrs until the end of the survival study. No difference in the effect of the treatment was observed in male versus female mice.

Histology

Harvested tissues were fixed in formalin (10%) for 24 hours before transfer to 70% ethanol followed by paraffinization and sectioning (7 μM). Slides were produced for tissue staining or stained with standard stains including H&E, for collagen deposition (Trichrome Stain Kit, MilliporeSigma), elastin (Verhoeff-Van Gieson, Thermo Fisher Scientific), or F-actin (ActinGreen 488 ReadyProbes, Thermo Fisher Scientific) for quantitative analysis. Elastin integrity score was rated by blinded observers and graded on an arbitrary scale of 5 (indicating high-quality elastic fiber) to 1 (indicating severe elastin fragmentation).

Blind test of aortic wall integrity

We first identified 2 independent participants who are familiar with aortic anatomy. Then we developed a comprehensive range of sections with a standardized score from 0 for the most calcified tissue where the elastin fibers are not present to 100% where elastin fibers within the aorta are visible with no sign of fragmentation. Next, images representing various levels of integrity were randomly assigned to the participants and data was collected for further analysis and data representation.

METHODS DETAILS

Human aortic tissue and calciphylaxis tissue

Human aortic tissue samples were collected from surgical specimens and through rapid autopsy of individuals within 4 hours of cardiac arrest. Aortic tissue was collected by a primary surgeon and were snap frozen. Skin tissue samples from calciphylaxis and control patients were obtained from Dr. Sagar Nigwekar, principal investigator of the Partners Calciphylaxis Biorepository and Patient Registry (ClinicalTrials.gov ID:NCT03032835). Both aortic (n = 4) and skin (n = 4) samples were collected at the Massachusetts General Hospital. Control aortic tissue (n = 3) was obtained from patients undergoing orthotopic cardiac transplant. IRB permissions do not allow for demographic information from discarded tissue to be collected or stored. All tissue samples were collected in compliance with the Mass General Brigham Institutional Review Board (IRB) requiring written informed consent.

Human coronary artery tissue procurement

Ischemic human coronary artery tissue biospecimens were obtained at Stanford University from diseased heart transplant donors consenting for research studies. Hearts were arrested in cardioplegic solution and transported on ice prior to dissecting proximal coronary artery segments from main branches of left anterior descending, circumflex or right coronary arteries. Epicardial and perivascular adipose was trimmed on ice, rinsed in cold phosphate buffered saline, and rapidly frozen in liquid nitrogen, and stored at -80°C. Normal human coronary artery tissue biospecimens were also obtained at Stanford University from non-diseased donor hearts rejected for orthotopic heart transplantation processed following the same protocol as hearts for transplant. Tissues were de-identified and clinical and histopathology information was used to classify ischemic and non-ischemic arteries. All normal arteries originated from hearts with left ventricular ejection fraction (LVEF) greater than 50%. Frozen tissues were transferred to the University of Virginia through a material transfer agreement (PI Dr. Miller) and Institutional Review Board approved protocols.

Coronary artery RNA extraction, QC, library construction and sequencing

Total RNA was extracted from frozen coronary artery segments using the Qiagen miRNeasy Mini RNA Extraction kit (catalog #217004). Approximately 50 mg of frozen tissue was pulverized using a mortar and pestle under liquid nitrogen. Tissue powder was then further homogenized in Qiazol lysis buffer using stainless steel beads in a Bullet Blender (Next Advance) homogenizer, followed by column-based purification. RNA concentration was determined using Qubit 3.0 and RNA quality was determined using Agilent 4200 TapeStation. Samples with RNA Integrity Number (RIN) greater than 5.5 and Illumina DV200 values greater than 75 were including for library construction. Total RNA libraries were constructed using the Illumina TruSeq Stranded Total RNA Gold kit (catalog #20020599) and barcoded using Illumina TruSeq RNA unique dual indexes (catalog # 20022371). After re-evaluating library quality using TapeStation, individually barcoded libraries were sent to Novogene for next generation sequencing. After passing additional QC, libraries were multiplexed and subjected to paired end 150 bp read sequencing on an Illumina NovaSeq S4 Flowcell to a median depth of 100 million total reads (>30 G) per library.

Coronary artery RNA-seq processing and analysis

The raw passed filter sequencing reads obtained from Novogene were demultiplexed using the bcl2fastq script. The quality of the reads was assessed using FASTQC and the adapter sequences were trimmed using trim galore. Trimmed reads were aligned to the hg38 human reference genome using STAR v2.7.3a according to the GATK Best Practices for RNA-seq. To increase mapping efficiency and sensitivity, novel splice junctions discovered in a first alignment pass with high stringency, were used as annotation in a second pass to permit lower stringency alignment and therefore increase sensitivity. PCR duplicates were marked using Picard, and WASP was used to filter reads prone to mapping bias. Total read counts and RPKM were calculated with RNA-SeQC v1.1.8 using default parameters and additional flags "-n 1000 -noDoC -strictMode" and GENCODE v30 reference annotation. The transcript and isoform expression levels were estimated using the RSEM package.

Coronary artery differential gene expression analysis

Differential gene expression analysis was performed on a subset of normal coronary artery (n = 24) and ischemic coronary artery (n = 36) raw read counts using DEseq2 (v3.1) after correcting for age, sex, RIN Score, ethnicity and hidden confounding variables (surrogate variables). Surrogate variables in the RNA-seq data were estimated in sva v3.2.0. These variables were then adjusted in DEseq2 along with other covariates. Differentially-expressed genes were called at FDR <0.05 significance cut-off, which identified more than 2300 upregulated and 1400 downregulated protein coding genes. P-values were adjusted for multiple testing using the Benjamini & Hochberg method.

Aortic smooth muscle cell lines

Primary human aortic vascular smooth muscle cells (VSMC) were purchased from Cell Applications Inc. (354K-05a), California, USA. To preserve cell identity all experiments were carried out at passages 1-5. Vascular smooth muscle cell identity (contractile phenotype) was assessed by immunofluorescence staining of contractile markers including SM22α, Calponin-1, and MYH11.

In vitro model of VSMC calcification

To induce calcification, VSMCs at 40% confluence were treated with DMEM supplemented with 10% fetal bovine serum, 10 mM β-glycerophosphate disodium, 50 μg/mL L-ascorbic acid, and 10 nM dexamethasone, as we previously described for 12 days.[28] To detect calcification, cells were fixed in 10% formalin and incubated with Alizarin Red at 2% (pH 4.1-4.3) for 10-20 min followed by 3x washing step with distilled water. For GSK343 treatment *in vitro*, VSMCs were supplemented with osteogenic media containing DMSO (0.05%) or GSK343 (15uM) for 12 days. Fresh media containing DMSO or GSK343 was applied every 2 days. For ULK1 inhibition *in vitro* VSMCs were sit in 12 well plates under osteogenic conditions containing SBI-0206965 inhibitor (iULK1) at 4, 8 and 12uM for 10 days followed by fixation and Alizarin red staining. For *in vivo* inhibition of ULK1, fresh living aortas from wild-type mice were incubated under osteogenic conditions containing SBI-0206965 inhibitor (iULK1) at 12uM for 12 days. Media containing the drug was replaced every 48 hrs.

Immunoblotting

Protein lysates were extracted using RIPA buffer (ThermoFisher, CA, USA) and supplemented with 1× of protease inhibitor cocktail (Roche) according to the manufacturer's instruction. 30 μg of total extracts were mixed with denaturing buffer (1× Laemmli loading buffer with 10% of β-mercaptoethanol) and analyzed by SDS–PAGE/western blot. Separated proteins were transferred onto a nitrocellulose membrane using the iBlot transfer system (Novex, ThermoFisher, USA). In general, primary antibodies were used at concentration of 1:100 and secondary antibodies at a concentration of 1:10000.

RNA isolation and RNA-seq analysis

Total RNA was extracted using a miRNeasy kit (Qiagen, Cat. No. / ID: 217084) following the manufacturer's protocol. For RNA-seq, we used the BGISEQ platform, on average generating about 4.28G bases per sample. The average alignment ratio with the reference genome was 97.01%, and the average mapping of the gene set was 74.05%. A total of 17029 genes were detected. We used HISAT to align the clean reads to the reference genome and Bowtie2 to align the clean reads to the reference genes. For qPCR, 100 ng of total RNA was used as the starting template for cDNA synthesis. The cDNA was prepared by reverse transcription (RT), and gene expression was analyzed by quantitative PCR (qPCR) on a SYBR green system (Applied Biosystems). Expression results were analyzed by the DDCT method, and GAPDH (encoding glyceraldehyde-3- phosphate dehydrogenase) was used as a housekeeping gene. Fold changes were calculated as the average relative to control cells growing in normal media.

ATAC-seq

1 million cells were plated under normal or osteogenic media containing DMSO or GSK343 for 12 days as described above. The ATAC-seq analysis was performed by Active Motif company (https://www.activemotif.com/blog-atac-seq) using the following protocol, as previously described.[24] Briefly, to prepare nuclei, 1 million cells were spun at 500 × g for 5 minutes, followed by a wash using 1000 μL of cold 1x PBS Then, cells were lysed using cold lysis buffer (10 mM Tris-Cl, pH 7.4, 10 mM NaCl, 3 mM MgCl2 and 0.1% IGEPAL CA-630) followed by 10 min of centrifugation at 500x. The transposition reaction was carried out for 30 minutes at 37°C. For PCR, library fragments were amplified using 1x NEBnext PCR master mix and 1.25 μM of custom Nextera PCR primers.

FISH and immunofluorescence microscopy

Stellaris® FISH Probes recognizing human ULK1 (SMF-1082-5) and labeled with Quasar® 570-labeled oligos (Biosearch Technologies, Inc., Petaluma, CA) were hybridized to tissue samples, following the manufacturer's instructions available online at www.biosearchtech.com/stellarisprotocols. Two-dimensional and white light images were analyzed using ImageJ software.

Ex vivo models

Human and mouse tissue were freshly collected and placed in 6 well plates with normal or osteogenic media for 24hrs before treatments. Then samples were dissected to generate control and treated groups. For Alizarin red staining tissues were cultured with osteogenic media for 21 days followed by fixation with paraformaldehyde at 4% and stained with Alizarin red solution for 5 min. For MMPsense and Osteosense imaging, 50uL of the probe per mL of media were incubated overnight. Then tissues were washed with cold PBS twice for 5 min each. Image was acquired using LI-COR imaging system. For GSK343 treatment, tissue samples were incubated with normal or osteogenic media containing 20uM of GSK343 or DMSO at 0.01% for 21 days. Fresh media containing GSK343 was provided every 48 hrs.

Collagen gel contraction assay

Treated cells were resuspended in normal or osteogenic media at 2-5 x 10^6 cells/mL, according to the manufacturer's instructions (CellBiollabs, USA). Then 0.5 mL of the cell-collagen mixture was polymerized. Next cells were incubated for two days under treatment conditions before releasing the stressed matrix. The collagen gel size change was measured using Image Pro Plus.

Calcium assay

Treated cells were resuspended in calcium assay buffer and sonicated on ice followed by centrifugation at 18000 rpm for 3min. Then supernatant was transferred to a 1.5 mL tube and mixed with the chromogenic reagent according to the manufacturer's protocol (Abcam, USA). Samples were read using a colorimetric microplate reader using OD575nm filter.

QUANTIFICATION AND STATISTICAL ANALYSIS

Summary-based Mendelian randomization analysis

Gene-level prioritization of calcification GWAS variants was performed using summary-based Mendelian Randomization (SMR).[44] GWAS summary statistics were obtained from the Cohorts for Heart and Aging Research in Genome Epidemiology (CHARGE) consortium on thoracic aortic calcification (TAC) from 8422 European ancestry individuals.[28] These data were integrated with cis-eQTL summary data from the Stockholm-Tartu Atherosclerosis Reverse Network Engineering Task (STARNET) containing atherosclerotic aortic root (AOR) and mammary artery (MAM) tissues derived from ~600 European individuals.[20] We used SMR to test the pleiotropic association of top TAC associated SNPs with gene expression in the STARNET eQTL datasets, as done previously.[20] We used the post-hoc heterogeneity in dependent instruments (HEIDI) test[44] to exclude loci with evidence of linkage or heterogeneity in the genetic instruments (P¬HEIDI < 0.01) rather than pleiotropy using the 1000G European LD reference panel. We considered only genes with at least 1 cis-eQTL p-value < 5E-5 for colocalization.

Activity-by-contact (ABC) enhancer-gene analysis

We used peripheral artery disease (PAD) GWAS summary data from the Million Veteran Program (MVP) meta-analysis with variants subset to suggestive associations (P<5E-05) to intersect with genome-wide enhancer-gene predictions calculated using the activity-by-contact (ABC) model. We used both the ENCODE coronary artery tissue and human coronary artery smooth muscle cell-based annotations from H3K27ac histone modification ChIP-seq and chromatin accessibility (ATAC-seq) datasets, and we considered significant enhancer-gene predictions with ABC scores > 0.02, as previously described. Interaction windows were defined by HiC contact boundaries averaged across multiple human tissues.

Statistics

Statistical analysis for *in vitro* and *in vivo* experiments was performed using Graph Pad Prism 8.0 (GraphPad Software, La Jolla, CA). Data are reported as mean ± SEM unless otherwise indicated. Two group comparisons of continuous variables were performed using the two-tailed Student t test. For more than 2-group comparisons of continuous variables, two-tailed one-way analysis of variance (ANOVA) with Sidak's test for multiple comparisons was used. For all experiments, at least 3 experimental replicates were performed. The Kaplan-Meier statistic with log-rank testing was used to compare survival of groups of mice. A two-tailed p<0.05 was considered to indicate statistical significance.